Nano Research

ISSN 1998-0124 CN 11-5974/O4
https://doi.org/10.1007/s12274-021-3419-2

Research Article

On-surface activation of benzylic C–H bonds for the synthesis of pentagon-fused graphene nanoribbons

Xiushang Xu[1,3,§], Marco Di Giovannantonio[2,†,§], José I. Urgel[2,‡], Carlo A. Pignedoli[2], Pascal Ruffieux[2], Klaus Müllen[1,4] (✉), Roman Fasel[2] (✉), and Akimitsu Narita[1,3] (✉)

[1] *Max Planck Institute for Polymer Research, 55128 Mainz, Germany*
[2] *Empa, Swiss Federal Laboratories for Materials Science and Technology, nanotech@surfaces Laboratory, 8600 Dübendorf, Switzerland*
[3] *Organic and Carbon Nanomaterials Unit, Okinawa Institute of Science and Technology Graduate University, 1919-1 Tancha, Onna-son, Kunigami-gun, Okinawa 904-0495, Japan*
[4] *Institute of Physical Chemistry, Johannes Gutenberg University Mainz, Duesbergweg 10-14, 55128 Mainz, Germany*
[†] *Present address: Istituto di Struttura della Materia-CNR (ISM-CNR), via Fosso del Cavaliere 100, 00133 Roma, Italy*
[‡] *Present address: IMDEA Nanoscience, C/Faraday 9, Campus de Cantoblanco, 28049 Madrid, Spain*
[§] *Xiushang Xu and Marco Di Giovannantonio contributed equally to this work.*

Received: 15 January 2021 / **Revised:** 21 February 2021 / **Accepted:** 23 February 2021

ABSTRACT

Graphene nanoribbons (GNRs) have potential for applications in electronic devices. A key issue, thereby, is the fine-tuning of their electronic characteristics, which can be achieved through subtle structural modifications. These are not limited to the conventional armchair, zigzag, and cove edges, but also possible through incorporation of non-hexagonal rings. On-surface synthesis enables the fabrication and visualization of GNRs with atomically precise chemical structures, but strategies for the incorporation of non-hexagonal rings have been underexplored. Herein, we describe the on-surface synthesis of armchair-edged GNRs with incorporated five-membered rings through the C-H activation and cyclization of benzylic methyl groups. *Ortho*-Tolyl-substituted dibromobianthryl was employed as the precursor monomer, and visualization of the resulting structures after annealing at 300 °C on a gold surface by high-resolution noncontact atomic force microscopy clearly revealed the formation of methylene-bridged pentagons at the GNR edges. These persisted after annealing at 340 °C, along with a few fully conjugated pentagons having singly-hydrogenated apexes. The benzylic methyl groups could also migrate or cleave-off, resulting in defects lacking the five-membered rings. Moreover, unexpected and unique structural rearrangements, including the formation of embedded heptagons, were observed. Despite the coexistence of different reaction pathways that hamper selective synthesis of a uniform structure, our results provide novel insights into on-surface reactions en route to functional, non-benzenoid carbon nanomaterials.

KEYWORDS

graphene nanoribbons, on-surface synthesis, scanning-tunneling microscope, noncontact atomic force microscope, C–H activation

1 Introduction

Graphene nanoribbons (GNRs) are a new class of next-generation carbon nanomaterials and have attracted widespread attention due to their unique electronic and magnetic properties. Their electronic band structures are critically depending upon structural features such as width, length and edge-types [1–4]. Precision synthesis of GNRs appears as a major challenge. To this end, on-surface synthesis based on the polymerization and planarization of tailor-made molecular precursors on metal surfaces under ultrahigh vacuum (UHV) conditions appears particularly powerful and offers the additional advantage of *in-situ* monitoring by atomic-resolution scanning probe microscopy [5–10]. Since the initial demonstration of 7-atom-wide armchair-type GNRs (7-AGNRs) on a Au(111) surface using 10,10'-dibromo-9,9'-bianthryl (DBBA) as a precursor [11], a range of GNRs with different structures have been prepared via on-surface synthesis, such as armchair GNRs (*N*-AGNRs) with different widths *N* (*N* = 5, 6, 8, 9, 10, 13, 15 and 17) [12–19], zigzag GNRs (ZGNRs) [20], chevron-type GNRs [11, 21], chiral (3,1)-GNRs containing zigzag and armchair edges [22], and heteroatom-doped GNRs with boron, nitrogen, oxygen, or sulfur [23–30]. π-Extension of 7-AGNRs through aryl-substitution of DBBA turned out to be of special value. Fischer, Crommie and co-workers demonstrated a synthesis of 13-AGNRs **1** (Fig. 1) using bis(biphenylyl)-substituted DBBA as the monomer [16]. A thiophene-incorporating 13-AGNR analogue was also achieved through (2-phenyl)thiophenyl-substitution of DBBA [31]. Moreover, naphtho-fused 7-AGNR **2** was synthesized by Moreno, Mugarza, and co-workers, using diphenyl-substituted DBBA [32], which formed superlattice arrays and could be further fused laterally to provide nanoporous graphene [33]. GNRs comprising not only carbon hexagons, but also sequences of 5-6-7 carbon rings and 4-5-7 rings were

Address correspondence to Klaus Müllen, muellen@mpip-mainz.mpg.de; Roman Fasel, Roman.Fasel@empa.ch; Akimitsu Narita, akimitsu.narita@oist.jp

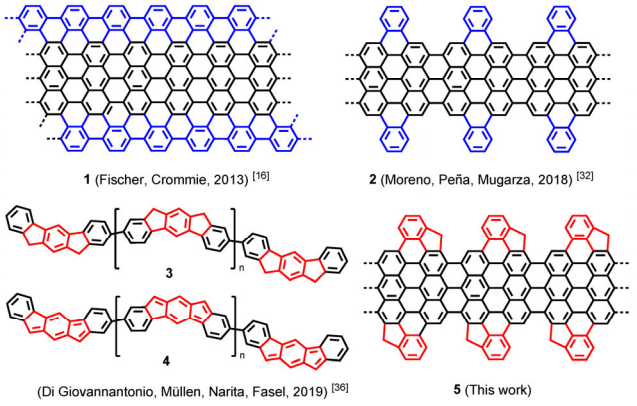

Figure 1 Molecular structures of 13-AGNR **1** and naphtho-fused 7-AGNR **2** previously prepared from aryl-substituted DBBA as precursors, dihydroindenofluorene and indenofluorene polymers **3** and **4**, respectively, and the pentagon-fused 7-AGNR **5** obtained in this work.

demonstrated by Gottfried and colleagues through fusion of 2,6-polyazulene chains [34], and indeno-fused 6-ZGNR was obtained via cyclization of phenyl rings against the zigzag edges, forming five-membered rings [20]. Nevertheless, there are only few established synthetic strategies to prepare GNRs incorporating non-hexagonal rings.

We have recently achieved on-surface syntheses of dihydroindenofluorene and indenofluorene polymers **3** and **4** (Fig. 1), respectively, through C–H activation of benzylic methyl groups installed on polyphenylenes, leading to the formation of five-membered rings with methylene- and methine-bridges [35–37]. We thus considered the structural extension of AGNR edges with five-membered rings by employing the same concept. To this end, we designed 10,10'-dibromo-2,2'-di-*ortho*-tolyl-9,9'-bianthracene (**12**) as a precursor monomer for naphtho-fused 7-AGNRs with additional five-membered rings. In this work, we report a synthesis of monomer **12** in solution, followed by on-surface fabrication of GNRs using **12** on a Au(111) surface under UHV conditions (Scheme 1). Upon thermal treatment at 300 °C, high-resolution noncontact atomic force microscopy (nc-AFM) revealed formation of pentagon-fused GNR **5** with methylene bridges, although a few fully conjugated five-membered rings with methine bridges as well as some defects due to migration and cleavage of the methyl groups were

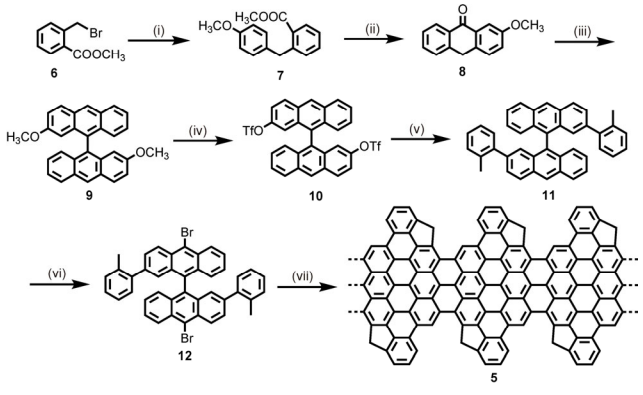

Scheme 1 Synthetic route to pentagon-fused GNR **5**. Reagents and conditions: (i) (4-methoxyphenyl)boronic acid, $Pd(PPh_3)_4$, Cs_2CO_3, 1,2-dimethoxyethane/H_2O, reflux, overnight, 78%; (ii) trifluoromethanesulfonic acid, CH_2Cl_2, room temperature, 12 h, 86%; (iii) Zn, $ZnCl_2$, THF/H_2O, room temperature, 48 h; then p-toluenesulfonic acid, toluene, 120 °C, 2 h, 35%; (iv) BBr_3 (1 M), CH_2Cl_2, room temperature, 12 h; then pyridine, Tf_2O, CH_2Cl_2, room temperature, 3 h, 70%; (v) *ortho*-tolylboronic acid, $Pd_2(dba)_3$, SPhos, K_3PO_4, toluene, 105 °C , 12 h, 78%; (vi) *N*-bromosuccinimide, CH_2Cl_2, room temperature, 24 h, 79%; (vii) Au(111), 300–340 °C.

also observed. Interestingly, azulene-incorporated structures were also detected, pointing to unexpected skeletal rearrangements probably induced by C-H activation of the benzylic methyl groups. Our results furnish unprecedented insights into on-surface reactivity of benzylic methyl groups, which are known to play an indispensable role in solution chemistry [38, 39]. The purpose of the present paper is to demonstrate their wide potential for achieving novel carbon nanostructures on surfaces.

2 Results and discussions

For the synthesis of precursor **12**, methyl 2-(4-methoxybenzyl)benzoate (**7**) was initially made by Suzuki-Miyaura coupling of methyl 2-(bromomethyl)benzoate (**6**) and 4-methoxyphenyl boronic acid in 74% yield. Subsequently, **7** was cyclized by trifluoromethanesulfonic acid to afford methoxyanthracen-9(10H)-one (**8**) in 86% yield. After the reductive coupling of **8** promoted by Zn, dehydroxylation in the presence of trifluoromethanesulfonic acid afforded 2,2'-dimethoxy-9,9'-bianthracene (**9**) in 35% yield. Then, **9** was subjected to demethylation by boron tribromide (BBr_3) in CH_2Cl_2 at 0 °C. The resulting 2,2'-dihydroxy-9,9'-bianthracene was reacted with trifluoromethanesulfonic anhydride (Tf_2O) to form bistriflate **10** in 70% yield. Suzuki-Miyaura coupling of **10** with *ortho*-tolylboronic acid gave the 2,2'-di-*ortho*-tolyl-9,9'-bianthracene (**11**). Finally, monomer **12** was produced by bromination of **11** by *N*-bromosuccinimide (NBS) at room temperature in 79% yield, and characterized by ^1H and ^{13}C NMR spectroscopy and high-resolution mass spectrometry (see the Electronic Supplementary Material (ESM)).

For the on-surface synthesis of the pentagon-fused AGNRs, monomer **12** was first sublimed onto a Au(111) substrate held at room temperature under UHV conditions. Annealing to 300 °C induced polymerization of **12** via homolytic cleavage of the C-Br bonds to generate diradical intermediates, followed by oxidative cyclodehydrogenation to provide planarized GNRs (apparent height of 2.0 Å with V_b = −0.1 V), as revealed by scanning tunneling microscopy (STM) (Fig. 2(a) and Fig. S1(a) in the ESM). Some randomly distributed bright protrusions (apparent height of 3.2 Å) were also observed, which we attribute to the presence of unreacted tolyl groups that induce a certain degree of non-planarity due to steric repulsion with the proton within the same bay region. To unambiguously identify the chemical structure of the planar segments of the observed GNRs, we recorded constant-height frequency-shift nc-AFM images with a CO-functionalized tip [40] (Figs. 2(b), 2(c), 2(e), and 2(f)). These images clearly reveal the presence of five-membered rings, confirming the on-surface C–H activation of the benzylic methyl groups to form C–C bonds with the sp^2 carbons of the GNR edges in the same bay regions. Many of the apexes of these five-membered rings appear brighter in nc-AFM imaging mode, which can be attributed to methylene bridges (–CH_2–), as previously reported [20, 36], corresponding to GNR **5**, while very few five-membered rings with singly hydrogenated methine bridges have also been observed (Figs. 2(b)–2(d)).

The nc-AFM images also display structural features that deviate from the ones expected for GNR **5** (Fig. 2). We could clearly identify the bare and methyl-substituted naphtho-fused edges (A and B in Fig. 2(g)) resulting from the removal and migration of methyl groups, respectively. We note that methyl groups are imaged as bright protrusions at 2.1 ± 0.1 Å away from the closest carbon atom of the GNR backbone, in agreement with the literature [41]. On the other hand, CO molecules are sometimes observed, located at variable distances from the

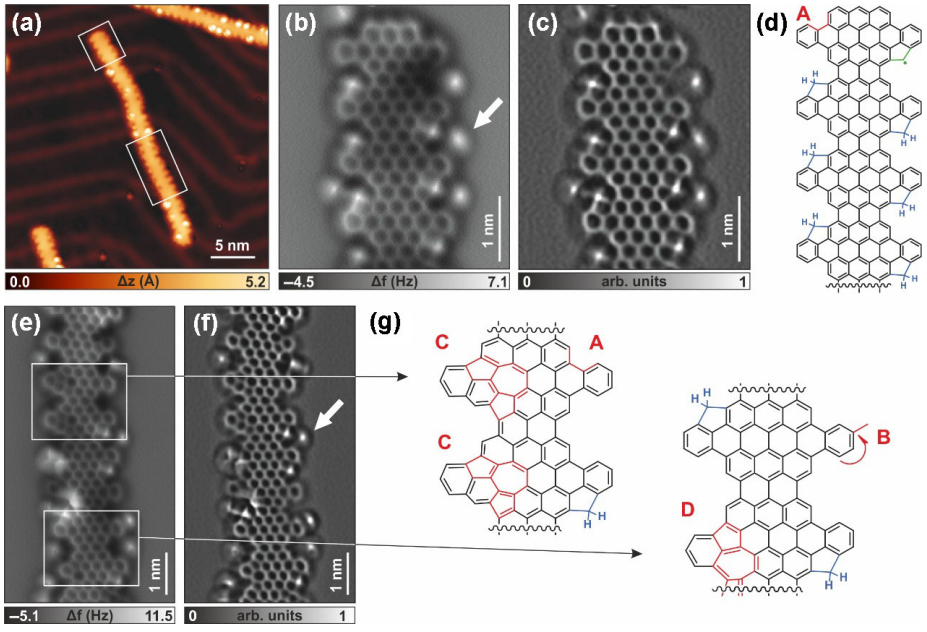

Figure 2 On-surface reaction of monomer **12** to pentagon-fused GNR **5**. (a) STM image after deposition of precursor **12** on Au(111) held at room temperature and subsequently annealed to 300 °C. ((b) and (e)) Constant-height frequency-shift nc-AFM images acquired with a CO-functionalized tip of the ribbon segments highlighted in panel (a). ((c) and (f)) Laplace-filtered images of panels (b) and (e). White arrows indicate CO molecules adsorbed next to the ribbons. (d) Chemical scheme of the structure observed in panel (b). (g) Chemical structures of some units of the ribbon in panel (e). The blue and green highlights represent the methylene and methine bridges, respectively, while the red highlights indicate the result of different types of chemical reactions involving the edges of the ribbons, which produce the structures labeled A–D. Scanning parameters: (a) V_b = −100 mV, I_t = 30 pA; (b) Δz = +220 Å with respect to STM set point: V_b = −5 mV, I_t = 100 pA; (e) Δz = +185 Å with respect to STM set point: V_b = −5 mV, I_t = 100 pA.

GNR (from 3.8 ± 0.1 to 4.4 ± 0.1 Å). Moreover, occasional skeletal rearrangements are revealed, affording different arrays of five-seven-five-membered rings with azulene substructures (C and D in Fig. 2(g)). In particular, the structural feature C demonstrates the formation of a seven-membered ring fully embedded inside the GNR structure, which has rarely been achieved via on-surface synthesis [34, 42].

Further annealing to 320 and 340 °C (Fig. S1 in the ESM) resulted in a gradual disappearance of the bright protrusions with apparent height of 3.2 Å, which we tentatively assigned to unreacted tolyl groups. These observations suggest planarization of the unreacted tolyl groups at higher temperatures, in line with similar reports in the literature [33]. After the heating step at 340 °C, almost completely planar GNRs could be obtained (apparent height of 2.0 Å in STM imaging, Fig. 3(a)). While standard STM imaging was not capable of elucidating the precise chemical structure of these GNRs, nc-AFM investigation of some segments of the obtained GNRs revealed similar structural features (Figs. 3(b) and 3(d)) as those observed after the 300 °C annealing (Fig. 2). The presence of five-membered rings with methylene bridges is evidenced by brighter protrusions at their apexes compared with a few fully conjugated pentagons (Figs. 3(b) and 3(d)), indicating that the dehydrogenation of the methylene groups did not efficiently proceed. The slight asymmetry of the five-membered rings in Fig. 3 is attributed to tip asymmetries [43]. Two five-membered rings were sometimes observed on the same side of a repeating unit along the GNR backbone, as a result of methyl migration (Fig. 3(c), central unit). A proper statistical analysis of the occurrence of pentagons with methylene or methine bridges and of the other different structural features observed could not be conducted due to the limited number of GNR segments imaged by nc-AFM, while standard STM images do not allow to unambiguously identify the relevant structural details. However, we could clearly identify the frequent cleavage of benzylic methyl groups from STM images taken after annealing at 300 °C as well as 340 °C,

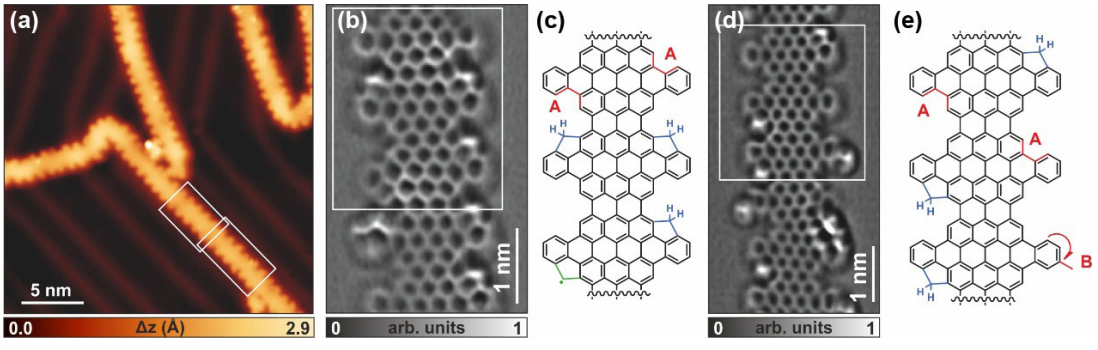

Figure 3 Scanning probe investigation of samples after annealing to 340 °C. (a) STM image after deposition of precursor **12** on Au(111) held at room temperature and subsequent annealing to 340 °C. ((b) and (d)) Laplace-filtered nc-AFM images of the ribbon segments highlighted in panel (a). The raw nc-AFM images are reported in Fig. S2 in the ESM. ((c) and (e)) Chemical structures of the parts highlighted with white frames. The blue and green highlights represent the methylene and methine bridges, respectively. Detachment and migration of methyl groups is observed to give rise to structures indicated by labels A and B, respectively. Scanning parameters: (a) V_b = −30 mV, I_t = 20 pA; (b) Δz = +190 Å with respect to STM set point: V_b = −5 mV, I_t = 100 pA; (d) Δz = +200 Å with respect to STM set point: V_b = −5 mV, I_t = 100 pA.

suggesting the necessity of lowering the C–H activation energy to achieve more selective synthesis of pentagon-fused GNRs.

To characterize the electronic properties of GNR **5**, we performed density functional theory (DFT) calculations in gas phase (Fig. 4). These calculations reveal dispersive bands in the band structure of GNR **5**, with a relatively small band gap of 0.74 eV. The five-membered rings with methylene bridges do not contribute to the conjugation (Figs. 4(a)–4(c)). The electronic properties of GNR **5** are thus expected to be very similar to those reported for GNR **2** (whose gas-phase structure is reported to have a DFT band gap of 0.74 eV) [33]. On the other hand, dehydrogenation of GNR **5** to GNR **13** (Fig. 4(f)) would drastically change the electronic properties of the GNR, because the carbon atoms at the apexes of five-membered rings would participate in π-conjugation. Such modification introduces two new bands in the calculated band structure of GNR **13** (Figs. 4(f)–4(j)), which reduces the band gap of the freestanding GNR to 0.41 eV.

3 Conclusion

In conclusion, we synthesized 10,10'-dibromo-2,2'-di-*ortho*-tolyl-9,9'-bianthracene (**12**) as a precursor of pentagon-fused GNRs and demonstrated the on-surface activation of the benzylic C–H bonds coupling against the GNR edges towards formation of GNR **5** incorporating methylene-bridged five-membered rings. We found GNR **5** to coexist with structural variations involving fully conjugated pentagons with methine bridges as well as products resulting from migration and cleavage of methyl groups. Careful investigation of the chemical structures by nc-AFM with CO-functionalized tips further revealed azulene-incorporating non-benzenoid substructures with five- and seven-membered rings, including an intriguing structural feature with a seven-membered ring completely embedded inside the GNR backbone. Although the formation of GNR **5** lacked selectivity, the detailed information obtained on the on-surface activation of benzylic C–H bonds and the resulting GNR structures are instructive to expand the scope of the on-surface synthesis approach. An overarching goal is the further optimization of monomer design in order to enhance the structural precision of GNRs which is, indeed, seen in other cases.

4 Experimental

4.1 Monomer synthesis and characterizations

All the experimental details for the synthesis of monomer **12** and characterizations of new compounds are reported in the ESM.

4.2 STM and nc-AFM experiments

The on-surface synthesis experiments were performed under UHV conditions with base pressure below 2×10^{-10} mbar. Au(111) substrates (MaTeck GmbH) were cleaned by repeated cycles of Ar+ sputtering (1 keV) and annealing (470 °C). The precursor molecules were thermally sublimated onto the clean Au(111) surface from quartz crucibles heated at 250 °C, which

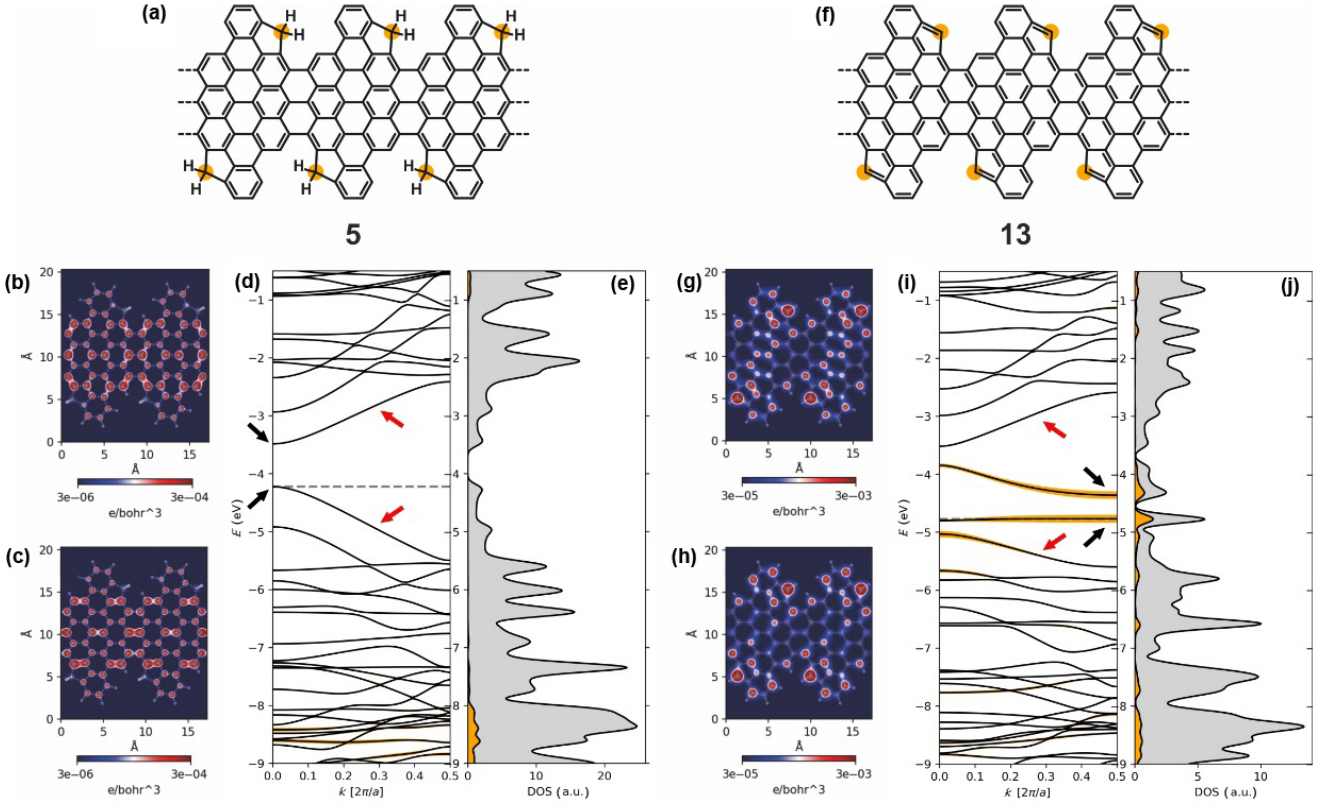

Figure 4 DFT study of the freestanding GNRs **5** and **13**. ((a), (f)) Chemical structures of GNR **5** and **13**, respectively. ((b), (c)) Spatial mapping of the frontier states corresponding to the bands and k points indicated by the black arrows in panel (d). ((d), (e)) Band structure and PDOS of GNR **5** with a band gap of 0.74 eV. ((g), (h)) Spatial mapping of the frontier states corresponding to the bands and k points indicated by the black arrows in panel i. ((i), (j)) Band structure and PDOS of GNR **13** with a band gap of 0.41 eV. In addition to the frontier bands observed for GNR **5** (red arrows in panels (d) and (i)), GNR **13** presents two new frontier bands. These new bands host states localized on the carbon atoms at the apexes of the five-membered rings, as demonstrated by the projection of the electronic states of the ribbon on atomic orbitals centered on these carbon atoms (orange highlights). In the case of GNR **5**, these carbon atoms are sp^3 hybridized and do not contribute to the frontier orbitals. The grey dashed line indicates the Fermi level. Both systems are non-magnetic, at the DFT level of theory with PBE approximation for the exchange correlation functional.

resulted in a deposition rate of ~ 0.5 Å·min^{-1}. STM images were acquired with a low-temperature scanning tunneling microscope (Scienta Omicron) operated at 4.7 K in constant-current mode using an etched tungsten tip. Bias voltages are given with respect to the sample. nc-AFM measurements were performed at 4.7 K with a tungsten tip placed on a qPlus tuning fork sensor [44]. The tip was functionalized with a single CO molecule at the tip apex picked up from the previously CO-dosed surface [45]. The sensor was driven at its resonance frequency (24,700 Hz) with a constant amplitude of 70 pm. The frequency shift from resonance of the tuning fork was recorded in constant-height mode using Omicron Matrix electronics and HF2Li PLL by Zurich Instruments. The Δz is positive (negative) when the tip-surface distance is increased (decreased) with respect to the STM set point at which the feedback loop is opened.

4.3 Computational methods

For the gas phase calculations of the infinite ribbons we used the Quantum Espresso package [46] and PAW pseudopotentials from the SSSP precision library [47]. A cutoff of 50 Ry and 400 Ry was used for the plane wave expansion of Kohn Sham orbitals and charge density, respectively. We used the PBE parameterization for the generalized gradient approximation of the exchange correlation functional. All calculations were performed within the AiiDA lab framework [48] based on AiiDA [49]. The full dataset of the calculations is available on the Materials Cloud archive [50].

Acknowledgements

We are grateful for the financial support by the Max Planck Society, the Swiss National Science Foundation under Grant No. 200020_182015, the NCCR MARVEL funded by the Swiss National Science Foundation (No. 51NF40-182892), the European Union's Horizon 2020 research and innovation programme under grant agreement number 785219 (Graphene Flagship Core 2), the Office of Naval Research (No. N00014-18-1-2708), and the Okinawa Institute of Science and Technology Graduate University (OIST). The Swiss National Supercomputing Centre (CSCS) under project ID s904 is acknowledged for computational resources. Skillful technical assistance by Lukas Rotach is gratefully acknowledged.

Funding note: Open access funding enabled and organized by Projekt DEAL.

Electronic Supplementary Material: Supplementary material (details of the synthesis and characterizations of all the new compounds; additional STM and nc-AFM images; NMR spectra) is available in the online version of this article at https://doi.org/10.1007/s12227-021-3419-2.

References

[1] Yano, Y.; Mitoma, N.; Ito, H.; Itami, K. A quest for structurally uniform graphene nanoribbons: Synthesis, properties, and applications. *J. Org. Chem*. **2020**, *85*, 4–33.

[2] Narita, A.; Wang, X. Y.; Feng, X. L.; Müllen, K. New advances in nanographene chemistry. *Chem. Soc. Rev*. **2015**, *44*, 6616–6643.

[3] Xu, X. S.; Müllen, K.; Narita, A. Syntheses and characterizations of functional polycyclic aromatic hydrocarbons and graphene nanoribbons. *Bull. Chem. Soc. Jpn*. **2020**, *93*, 490–506.

[4] Chen, Z. P.; Narita, A.; Müllen, K. Graphene nanoribbons: On-surface synthesis and integration into electronic devices. *Adv. Mater*. **2020**, *32*, 2001893.

[5] Clair, S.; de Oteyza, D. G. Controlling a chemical coupling reaction on a surface: Tools and strategies for on-surface synthesis. *Chem. Rev*. **2019**, *119*, 4717–4776.

[6] Dong, L.; Liu, P. N.; Lin, N. Surface-activated coupling reactions confined on a surface. *Acc. Chem. Res*. **2015**, *48*, 2765–2774.

[7] Niu, T. C.; Zhang, J. L.; Chen, W. Atomic mechanism for the growth of wafer-scale single-crystal graphene: Theoretical perspective and scanning tunneling microscopy investigations. *2D Mater*. **2017**, *4*, 042002.

[8] Shen, Q.; Gao, H. Y.; Fuchs, H. Frontiers of on-surface synthesis: From principles to applications. *Nano Today* **2017**, *13*, 77–96.

[9] Gross, L.; Schuler, B.; Pavliček, N.; Fatayer, S.; Majzik, Z.; Moll, N.; Peña, D.; Meyer, G. Atomic force microscopy for molecular structure elucidation. *Angew. Chem., Int. Ed*. **2018**, *57*, 3888–3908.

[10] Zhou, X. H.; Yu, G. Modified engineering of graphene nanoribbons prepared via on-surface synthesis. *Adv. Mater*. **2020**, *32*, 1905957.

[11] Cai, J. M.; Ruffieux, P.; Jaafar, R.; Bieri, M.; Braun, T.; Blankenburg, S.; Muoth, M.; Seitsonen, A. P.; Saleh, M.; Feng, X. L. et al. Atomically precise bottom-up fabrication of graphene nanoribbons. *Nature* **2010**, *466*, 470–473.

[12] Zhang, H. M.; Lin, H. P.; Sun, K. W.; Chen, L.; Zagranyarski, Y.; Aghdassi, N.; Duhm, S.; Li, Q.; Zhong, D. Y.; Li, Y. Y. et al. On-surface synthesis of rylene-type graphene nanoribbons. *J. Am. Chem. Soc*. **2015**, *137*, 4022–4025.

[13] Denk, R.; Hohage, M.; Zeppenfeld, P.; Cai, J. M.; Pignedoli, C. A.; Söde, H.; Fasel, R.; Feng, X. L.; Müllen, K.; Wang, S. D. et al. Exciton-dominated optical response of ultra-narrow graphene nanoribbons. *Nat. Commun*. **2014**, *5*, 4253.

[14] Basagni, A.; Sedona, F.; Pignedoli, C. A.; Cattelan, M.; Nicolas, L.; Casarin, M.; Sambi, M. Molecules–oligomers–nanowires–graphene nanoribbons: A bottom-up stepwise on-surface covalent synthesis preserving long-range order. *J. Am. Chem. Soc*. **2015**, *137*, 1802–1808.

[15] Talirz, L.; Söde, H.; Dumslaff, T.; Wang, S. Y.; Sanchez-Valencia, J. R.; Liu, J.; Shinde, P.; Pignedoli, C. A.; Liang, L. B.; Meunier, V. et al. On-surface synthesis and characterization of 9-atom wide armchair graphene nanoribbons. *ACS Nano* **2017**, *11*, 1380–1388.

[16] Chen, Y. C.; de Oteyza, D. G.; Pedramrazi, Z.; Chen, C.; Fischer, F. R.; Crommie, M. F. Tuning the band gap of graphene nanoribbons synthesized from molecular precursors. *ACS Nano* **2013**, *7*, 6123–6128.

[17] Abdurakhmanova, N.; Amsharov, N.; Stepanow, S.; Jansen, M.; Kern, K.; Amsharov, K. Synthesis of wide atomically precise graphene nanoribbons from *para*-oligophenylene based molecular precursor. *Carbon* **2014**, *77*, 1187–1190.

[18] Sun, K. W.; Ji, P. H.; Zhang, J. J.; Wang, J. X.; Li, X. C.; Xu, X.; Zhang, H. M.; Chi, L. F. On-surface synthesis of 8-and 10-armchair graphene nanoribbons. *Small* **2019**, *15*, 1804526.

[19] Yamaguchi, J.; Hayashi, H.; Jippo, H.; Shiotari, A.; Ohtomo, M.; Sakakura, M.; Hieda, N.; Aratani, N.; Ohfuchi, M.; Sugimoto, Y. et al. Small bandgap in atomically precise 17-atom-wide armchair-edged graphene nanoribbons. *Comms. Mater*. **2020**, *1*, 36.

[20] Ruffieux, P.; Wang, S. Y.; Yang, B.; Sánchez-Sánchez, C.; Liu, J.; Dienel, T.; Talirz, L.; Shinde, P.; Pignedoli, C. A.; Passerone, D. et al. On-surface synthesis of graphene nanoribbons with zigzag edge topology. *Nature* **2016**, *531*, 489–492.

[21] Costa, P. S.; Teeter, J. D.; Enders, A.; Sinitskii, A. Chevron-based graphene nanoribbon heterojunctions: Localized effects of lateral extension and structural defects on electronic properties. *Carbon* **2018**, *134*, 310–315.
[22] Han, P.; Akagi, K.; Federici Canova, F.; Mutoh, H.; Shiraki, S.; Iwaya, K.; Weiss, P. S.; Asao, N.; Hitosugi, T. Bottom-up graphene-nanoribbon fabrication reveals chiral edges and enantioselectivity. *ACS Nano* **2014**, *8*, 9181–9187.
[23] Miao, D. D.; Daigle, M.; Lucotti, A.; Boismenu-Lavoie, J.; Tommasini, M.; Morin, J. F. Toward thiophene-annulated graphene nanoribbons. *Angew. Chem., Int. Ed.* **2018**, *57*, 3588–3592.
[24] Wang, X. Y.; Urgel, J. I.; Barin, G. B.; Eimre, K.; Di Giovannantonio, M.; Milani, A.; Tommasini, M.; Pignedoli, C. A.; Ruffieux, P.; Feng, X. L. et al. Bottom-up synthesis of heteroatom-doped chiral graphene nanoribbons. *J. Am. Chem. Soc.* **2018**, *140*, 9104–9107.
[25] Kawai, S.; Saito, S.; Osumi, S.; Yamaguchi, S.; Foster, A. S.; Spijker, P.; Meyer, E. Atomically controlled substitutional boron-doping of graphene nanoribbons. *Nat. Commun.* **2015**, *6*, 8098.
[26] Cloke, R. R.; Marangoni, T.; Nguyen, G. D.; Joshi, T.; Rizzo, D. J.; Bronner, C.; Cao, T.; Louie, S. G.; Crommie, M. F.; Fischer, F. R. Site-specific substitutional boron doping of semiconducting armchair graphene nanoribbons. *J. Am. Chem. Soc.* **2015**, *137*, 8872–8875.
[27] Kawai, S.; Nakatsuka, S.; Hatakeyama, T.; Pawlak, R.; Meier, T.; Tracey, J.; Meyer, E.; Foster, A. S. Multiple heteroatom substitution to graphene nanoribbon. *Sci. Adv.* **2018**, *4*, eaar7181.
[28] Bronner, C.; Stremlau, S.; Gille, M.; Brauße, F.; Haase, A.; Hecht, S.; Tegeder, P. Aligning the band gap of graphene nanoribbons by monomer doping. *Angew. Chem., Int. Ed.* **2013**, *52*, 4422–4425.
[29] Zhang, Y. F.; Zhang, Y.; Li, G.; Lu, J. C.; Que, Y. D.; Chen, H.; Berger, R.; Feng, X. L.; Müllen, K.; Lin, X. et al. Sulfur-doped graphene nanoribbons with a sequence of distinct band gaps. *Nano Res.* **2017**, *10*, 3377–3384.
[30] Durr, R. A.; Haberer, D.; Lee, Y. L.; Blackwell, R.; Kalayjian, A. M.; Marangoni, T.; Ihm, J.; Louie, S. G.; Fischer, F. R. Orbitally matched edge-doping in graphene nanoribbons. *J. Am. Chem. Soc.* **2018**, *140*, 807–813.
[31] Nguyen, G. D.; Toma, F. M.; Cao, T.; Pedramrazi, Z.; Chen, C.; Rizzo, D. J.; Joshi, T.; Bronner, C.; Chen, Y. C.; Favaro, M. et al. Bottom-up synthesis of $N = 13$ sulfur-doped graphene nanoribbons. *J. Phys. Chem. C* **2016**, *120*, 2684–2687.
[32] Moreno, C.; Paradinas, M.; Vilas-Varela, M.; Panighel, M.; Ceballos, G.; Peña, D.; Mugarza, A. On-surface synthesis of superlattice arrays of ultra-long graphene nanoribbons. *Chem. Commun.* **2018**, *54*, 9402–9405.
[33] Moreno, C.; Vilas-Varela, M.; Kretz, B.; Garcia-Lekue, A.; Costache, M. V.; Paradinas, M.; Panighel, M.; Ceballos, G.; Valenzuela, S. O.; Peña, D. et al. Bottom-up synthesis of multifunctional nanoporous graphene. *Science* **2018**, *360*, 199–203.
[34] Fan, Q. T.; Martin-Jimenez, D.; Ebeling, D.; Krug, C. K.; Brechmann, L.; Kohlmeyer, C.; Hilt, G.; Hieringer, W.; Schirmeisen, A.; Gottfried, J. M. Nanoribbons with nonalternant topology from fusion of polyazulene: Carbon allotropes beyond graphene. *J. Am. Chem. Soc.* **2019**, *141*, 17713–17720.
[35] Di Giovannantonio, M.; Urgel, J. I.; Beser, U.; Yakutovich, A. V.; Wilhelm, J.; Pignedoli, C. A.; Ruffieux, P.; Narita, A.; Müllen, K.; Fasel, R. On-surface synthesis of indenofluorene polymers by oxidative five-membered ring formation. *J. Am. Chem. Soc.* **2018**, *140*, 3532–3536.
[36] Di Giovannantonio, M.; Eimre, K.; Yakutovich, A. V.; Chen, Q.; Mishra, S.; Urgel, J. I.; Pignedoli, C. A.; Ruffieux, P.; Müllen, K.; Narita, A. et al. On-surface synthesis of antiaromatic and open-shell indeno [2,1-*b*] fluorene polymers and their lateral fusion into porous ribbons. *J. Am. Chem. Soc.* **2019**, *141*, 12346–12354.
[37] Di Giovannantonio, M.; Chen, Q.; Urgel, J. I.; Ruffieux, P.; Pignedoli, C. A.; Müllen, K.; Narita, A.; Fasel, R. On-surface synthesis of oligo (indenoindene). *J. Am. Chem. Soc.* **2020**, *142*, 12925−12929.
[38] Yazaki, R.; Ohshima, T. Recent strategic advances for the activation of benzylic C-H bonds for the formation of C-C bonds. *Tetrahedron Lett.* **2019**, *60*, 151225.
[39] Xue, X. S.; Ji, P. J.; Zhou, B. Y.; Cheng, J. P. The essential role of bond energetics in C-H activation/functionalization. *Chem. Rev.* **2017**, *117*, 8622–8648.
[40] Gross, L.; Mohn, F.; Moll, N.; Liljeroth, P.; Meyer, G. The chemical structure of a molecule resolved by atomic force microscopy. *Science* **2009**, *325*, 1110–1114.
[41] Betancourt, S. S.; Johansen, Y. B.; Forsythe, J. C.; Rinna, J.; Christoffersen, K.; Skillingstad, P.; Achourov, V.; Canas, J.; Chen, L.; Pomerantz, A. E. et al. Gravitational gradient of asphaltene molecules in an oilfield reservoir with light oil. *Energy Fuels* **2018**, *32*, 4911– 4924.
[42] Lohr, T. G.; Urgel, J. I.; Eimre, K.; Liu, J. Z.; Di Giovannantonio, M.; Mishra, S.; Berger, R.; Ruffieux, P.; Pignedoli, C. A.; Fasel, R. et al. On-surface synthesis of non-benzenoid nanographenes by oxidative ring-closure and ring-rearrangement reactions. *J. Am. Chem. Soc.* **2020**, *142*, 13565–13572.
[43] Gross, L. Recent advances in submolecular resolution with scanning probe microscopy. *Nat. Chem.* **2011**, *3*, 273–278.
[44] Giessibl, F. J. Atomic resolution on Si(111)-(7 × 7) by noncontact atomic force microscopy with a force sensor based on a quartz tuning fork. *Appl. Phys. Lett.* **2000**, *76*, 1470–1472.
[45] Bartels, L.; Meyer, G.; Rieder, K. H.; Velic, D.; Knoesel, E.; Hotzel, A.; Wolf, M.; Ertl, G. Dynamics of electron-induced manipulation of individual CO molecules on Cu(111). *Phys. Rev. Lett.* **1998**, *80*, 2004–2007.
[46] Giannozzi, P.; Andreussi, O.; Brumme, T.; Bunau, O.; Nardelli, M. B.; Calandra, M.; Car, R.; Cavazzoni, C.; Ceresoli, D.; Cococcioni, M. et al. Advanced capabilities for materials modelling with QUANTUM ESPRESSO. *J. Phys.: Condens. Matter* **2017**, *29*, 465901.
[47] Prandini, G.; Marrazzo, A.; Castelli, I. E.; Mounet, N.; Marzari, N. Precision and efficiency in solid-state pseudopotential calculations. *npj Comput. Mater.* **2018**, *4*, 72.
[48] Yakutovich, A. V.; Eimre, K.; Schütt, O.; Talirz, L.; Adorf, C. S.; Andersen, C. W.; Ditler, E.; Du, D.; Passerone, D.; Smit, B. et al. AiiDAlab – an ecosystem for developing, executing, and sharing scientific workflows. *Comput. Mater. Sci.* **2021**, *188*, 110165.
[49] Pizzi, G.; Cepellotti, A.; Sabatini, R.; Marzari, N.; Kozinsky, B. AiiDA: Automated interactive infrastructure and database for computational science. *Comput. Mater. Sci.* **2016**, *111*, 218–230.
[50] Xu X. S.; Di Giovannantonio M.; Urgel, J. I.; Pignedoli, C. A.; Ruffieux, P.; Müllen, K.; Fasel, R.; Narita, A. On-surface activation of benzylic C-H bonds for the synthesis of pentagon-fused graphene nanoribbons. Materials Cloud Archive 2021.63 (2021), doi: 10.24435/materialscloud:xj-bb.